EUROPEAN SPALLATION SOURCE

ESS Instrument Construction Proposal
C-SPEC - Cold chopper spectrometer

	Name (name, title, e-mail address)	Affiliation (name of institution, address)
Proposer	Wiebke Lohstroh, Dr. , wiebke.lohstroh@frm2.tum.de	Technische Universität München Forschungsneutronenquelle Heinz Maier-Leibnitz (FRM II) Lichtenbergstraße 1 85747 Garching, Germany
Co-proposers	Winfried Petry, Prof. Dr., winfried.petry@frm2.tum.de Jürgen Neuhaus, Dr., juergen.neuhaus@frm2.tum.de Luca Silvi, Mr. luca.silvi@frm2.tum.de Christine Alba-Simionesco, Prof. christiane.alba-simionesco@cea.fr Jean-Marc Zanotti, Dr. jean-marc.zanotti@cea.fr Stephane Longeville stephane.longeville@cea.fr	Technische Universität München Forschungsneutronenquelle Heinz Maier-Leibnitz (FRM II) Lichtenbergstraße 1 85747 Garching, Germany Laboratoire Léon Brillouin C.E.A Saclay 91191 Gif-sur-Yvette Cedex, France
ESS coordinator	Pascale Deen	

Note: All proposals received by ESS will be included as Expressions of Interest for In-kind contributions. ESS will use this information for planning purposes and the proposer or affiliated organization is not obligated to materially contribute to the project.

The following table is used to track the ESS internal distribution of the submitted proposal.

	Name
Document submitted to	Ken Andersen
Distribution	Dimitri Argyriou, Oliver Kirstein, Arno Hiess, Robert Connatser, Sindra Petersson Årsköld, Richard Hall-Wilton, Phillip Bentley, Iain Sutton, Thomas Gahl, relevant STAP

ENCLOSURES

<< 131031_cspec_mcstas_lohstroh_v1.zip>>

EXECUTIVE SUMMARY

Many research fields and scientific questions of the future can best be addressed using a high performance direct geometry time-of-flight spectrometer. The areas of interest include biological and life sciences, soft condensed matter research, magnetic materials and novel quantum critical phenomena, or materials science and materials development. The questions to be addressed are driven by fundamental interest as well as technological relevance. Common to these seemingly diverse areas is the fact that the full understanding of their properties and functionalities requires a detailed understanding of their dynamics. Most prominently in biology: life depends on mobile water and with ceasing mobility of the water molecules all biological activity comes to a halt. Similarly, dynamic properties govern the response of stimuli responsive polymers, hydrogels, or of molecular liquids. Ideally, these materials will be studied while the external stimulus is applied (e.g pressure, electrical potential or similar) in dedicated pump-probe experiments. On the other hand, measurements of the excitation spectrum of novel magnetic materials are crucial for the understanding of the interaction potentials and to benchmark experiments with theory. Those questions will still be relevant in the coming years and the quest to answer them drives the development of the here proposed time-of-flight chopper spectrometer.

The science drivers that are briefly recapitulated above require experiments in the time domain ranging from pico- to nanoseconds. For that, the instrument is designed to cover an energy resolution of $\Delta E/E$ = 6 - 1% and it will utilize cold neutrons in the range from $\lambda = 1 - 20$ Å. Most experiments are expected to require settings of about 3% energy resolution (i.e. 100 µeV at $\lambda = 5$ Å) and the instrument performance is optimized for these values. In order to minimize effects of the asymmetric source pulse on the resolution function, the pulse needs to be shaped (with an optimum value of FWHM = 1000 µs). Assuming balanced operating conditions yields an optimum instrument length of 120.4 m (L_{PM}= 108 m) for the 3% $\Delta E/E$ setting. This instrument length permits a wavelength band of 2.5 Å at the detector position. The operation parameters of the chopper system enable the choice between single and multi energy mode, and the number simultaneous probed incoming energies E_i can be set according to the requirements of the experiment. In general, one order of magnitude of ΔE can be probed simultaneously in any experiment. If only a lower energy resolution is required, the full source pulse can be used in favour for higher intensity. Similarly, every second source pulse can be suppressed in favour for a larger band width.

The guide systems will have two configurations, i.e. a large homogeneous beam spot and a focussing option. It will be realized by an exchangeable guide section after the monochromatizing system. In this manner the divergent requirements of the science drivers can be accommodated: Hydrogenous materials and singles crystals benefit from a larger beam spot with homogenous flux distribution and low divergence while experiments with restricted sample sizes (either due to a limited amount of sample, or due to the sample environment restricting the access) are best investigated using a focussed beam. The guide system will be optimized for high flux in the cold region and the design avoids the direct line-of-sight to the source in order to obtain an excellent signal to noise ratio. The secondary spectrometer will have a flight path of 4 m and an angular coverage of -15 – 140°. A

reasonable side access of the sample area (of approximately 60°) is favoured over larger angular detector coverage as it facilitates the integration of more specialized sample equipment and secondary characterisation of the samples on-line. We expect an increasing demand of these kind of experiments in the coming years as there is a trend to investigate increasingly more complex samples which are technological more relevant. The dynamic range of the spectrometer will cover the relevant length scales required by the science drivers. I.e. the q-range should extend to low values ($q \leq 0.05$ Å^{-1}) for soft matter and biological applications whose characteristic length scales are often in the range of 10 - 1000 Å while on the other hand, large accessible momentum transfer values ($q \leq 10$ Å^{-1}) are required for materials science questions with length scales on the order of Ångströms. The latter can be ascertained by a significant flux of the incoming neutrons toward the thermal regime. Provisions for a small angle detector (together with a low divergence beam) will be made to be able to probe the low angle region.

The instrument concept relies on established and proven concepts, with the exception of the detector. With the shortage of ^{3}He-detector tubes, this is common for all ESS instruments that require a large area detector. The guide and chopper technology are established and with the technology available today, all the driving scientific questions can be addressed in an excellent manner. Suppose that the maturity of the currently developed ^{10}B-conversion layer detectors will sufficiently advance in the coming years, there is no major risk associated in building the instrument. It will serve a broad user community and significant advances in the field of biology, soft condensed matter, materials science and magnetic phenomena can be expected from day one of instrument operation.

TABLE OF CONTENTS

1.   INSTRUMENT PROPOSAL

1.1   Scientific Case

For the scientific challenges of the future, a multitude of different research fields will benefit from a cold direct geometry chopper spectrometer. The areas range from biological and soft matter materials, materials science questions or novel magnetic quantum materials. Common to these diverse fields is the fact that they all require an instrument capable to probe time scales from pico- to nanoseconds on a length scale from Ångström to nanometers. Moreover, there is a trend, and also the necessity, to investigate not only model systems but materials that are more realistic and hence technological more relevant. That often implies higher complexity of the investigated systems. This complexity can be for instance in composition when moving away from isolated substances to composites or crowed solutions. For a detailed understanding, the dynamic landscape needs to be probed over a large scale, i.e. it is mandatory to access different time domains experimentally. The proposed instrument will be ideally suited for exploring dynamical properties and especially in multi-energy mode, it will reduce the necessary measurement times considerably. More importantly, kinetic studies on samples that might change with time, temperature, etc. will benefit as it inherently guaranties identical sample conditions for each of the datasets. Another level of complexity occurs due to sample treatment or sample preparation during the experiment. Many technological relevant questions in the area of materials science are best addressed in *in-situ* experiments as it is routinely done e.g. for diffraction. Examples include phase transitions in Li-ion batteries during charging and discharging, heat treatment of new high strength alloys, phase transitions during gas adsorption in host-guest systems, or high pressure experiments on mulitferroic materials. With the new high flux instruments, the field of in-situ experiments

will be opened towards the inelastic and quasielastic domain and a significant impact to the development of new technologies can be expected. Alongside in-situ experiments, the possibility to include a secondary characterization during the experiment (e.g. Raman or infra-red spectroscopy, NMR) or pump-probe type experiments will further increase the understanding of dynamic processes. More specifically, the new instrument will make a significant impact for:

Biological applications:

Living cells are mainly comprised of water and without water there would be no biological activity. Proteins, peptides, enzymes or DNA always contain water molecules, and in living cells they are always surrounded by an aqueous environment. It is well understood that the proton dynamics in biological systems is correlated to biological activity. [1] E.g. for a number of proteins it has been demonstrated that the dynamical phase transition of the hydration shell water around 220 K is accompanied by ceasing biological activity [2] but the number of experiments that directly compare protein and hydration shell dynamics is still limited. [3] Generally, protein dynamics can occur on a wide range of time-scales, including fast dynamics side chain reorientation, slow conformational changes of the chains or stochastic motions [4] and their dynamics is intrinsically coupled to the functionality of the protein. As the samples of interest are moving from isolated model substances to more realistic and complex materials such as crowed solution a thorough understanding of the dynamics properties is essential but characterization also becomes more demanding. Although the cross section of the proton for incoherent scattering is high and thus neutron spectroscopy is a unique tool, experiments dedicated to biological topics are just at the beginning. Experimental sample sizes might be small and the signal of interest might be well concealed in the scattering originating from other parts of the sample, especially if partial deuteration proves difficult. With the concurrent characterization of such samples in many time domains at an instrument with excellent signal-to-noise ratio and a large q-range, the dynamics of different bound water populations can be probed in unprecedented detail and thus new insights in the interconnection of motion and dynamics in biological systems are to be expected. This will be aided by the advances in theoretical simulation techniques which can be expected to arise from more sophisticated models and more computer power. The high energy resolution option of the instrument enables to also explore the slow dynamics region to gain sufficient overlap with instruments dedicated to measure slow dynamics such as backscattering or neutron spin echo. Moreover, the possibility to couple pump-probe experiment with quasi elastic neutron scattering (QENS) and thus stimulate specific responses e.g. for light harvesting molecules promises great advances.

Soft condensed matter:

Soft condensed matter systems such as polymers, lipid membranes, or molecular liquids are prevailing in a number of technological important fields, e.g. pharmaceutical applications,

[1] H.E. Stanley S.V. Buldyrev, P. Kumar et al, *J. Non-crystalline solids* 357 (2011) 629-640.
[2] (a) G. Zaccai, *J. Non-crystalline Solids* 357 (2011) 615-621; (b) W. Doster, *J. Non-crystalline Solids* 357 (2011) 622-628, (c) W. Doster, S. Busch, A. M. Gaspar, et al, *Physical Review Letters*, 104 (2010) 098101; (d) J. Qvist, E. Persson, C. Mattea, and B. Halle, *Faraday Discussions*, 141 (2009) 131–144.
[3] J. D. Nickels H. O'Neill, L. Hong et al, *Biophysical Journal* 103 (2012) 1566-1575.
[4] J. Pieper and G. Renger, *Photosyth. Res* 102 (2009) 281-293.

gas and oil industry, manufacturing involving polymers and plastics or food industry. [5] Better understanding of the materials properties and the manufacturing processes thus has direct impact on the production economy. Typically, the dynamical properties on various time-scales will determine the materials properties [6], such as the response of in stimuli-responsive hydrogels [7], or transport properties in lipid layers. [8] The dynamic properties of soft condensed matter or disordered materials also play a crucial role in pharmaceutical applications. For instance, the dynamic properties of excipients (used to stabilize active pharmaceutical ingredients) were correlated to the deactivation time of the bioactive component [9] and thus directly influences shelf life of the drug. Besides a careful characterization of the starting material, it is also of interest to monitor potential alterations of the dynamic landscape incurred during processing (e.g. due to heat treatment, mechanical forces during mixing or tableting), and the possible interaction with the targeted molecules (such as proteins). It is also known that minor changes of the molecular structure of pharmaceuticals can have profound effects on the toxicity, solubility and the biological activity. All these properties can be interconnected with the dynamics of molecular fragments, hydrogen bonding in solution or in the solid [10] which can be probed by neutron quasielastic scattering and low frequency vibrational spectroscopy. With an instrument capable of mapping the dynamic landscape efficiently under realistic processing conditions further advances are to be expected in fundamental understanding and technological application.

Functional Materials and materials science

The understanding of atomic mobility on a microscopic level is a prerequisite for materials development. The examples are numerous and cover a wide range of different areas such as ultra high strength concrete [11], ion mobility in ionic liquid electrolytes [12], proton diffusivity in ceramic perovskites to be used as electrolyte membrane in fuel cells and water steam reformers [13], gas adsorption in porous materials for CO_2 sequestration, or diffusion dynamics in metal alloy melts. [14] For instance, in porous metal-organic framework systems (MOFs), the full understanding of the binding energy of guest molecules can help to tailor suitable MOFs for the intended application e.g. as H_2 storage materials. On the other hand transport properties of the guest molecules in such frameworks are import for filter applications e.g. separation of hydrocarbons [15]. Quasielastic scattering and low energy

[5] V. Sakai and A. Arbe, Current Opinion in Colloid & Interface Science 14 (2009) 381-390.

[6] C. Gerstl, G. J. Schneider, A. Fuxman et al, *Macromolecules*, 45 (2012) 4394–4405.

[7] (a) Ch. Chiapponi, M.T. Di Bari, Y. Gerelli et al, *J. Phys. Chem. B* 116 (2012) 12915-12921; (b) M-T. Popescu, C. Tsitsilianis, Ch. Papadakis et al, *Macromolecules* 45 (2012) 3523-3530.

[8] S. König, E. Sackmann, D. Richter et al, *J. Chem Phys.* 100 (1994) 3307-3316; A. Buchsteiner, Th. Hauss, S. Dante and N. A. Dencher, *Biochimica and Biophysica Acta* 1798 (2010) 1969-1976; S. Busch and T. Unruh, *Biochimica and Biophysica Acta* 1808 (2011) 199-208.

[9] M. T. Cicerone and Ch. L. Soles, *Biophysical journal* 86.6 (2004) 3836-3845.

[10] H. N. Bordallo, B. A. Zakharov, E. V. Boldyreva et al, *molecular pharmaceutics* 9 (2012), 2434-244.

[11] (a) H. N. Bordallo, L. P. Aldrige and A. Demedt, *J. Phys. Chem B* 110 (2006) 17966-17976; (b) T. Gutberlet, H. Hilbig, et al., *Cement and Concrete Research* 51 (2013) 104–108.

[12] (a) M. Kofu, M. Nagao, T. Ueki et al, *J. Phys. Chem B* 117 (2013) 2773-2781; (b) B. Aoun, M. A. González, J. Ollivier et al., *J. Phys. Chem. Letters* 1, (2010) 2503–2507.

[13] A. Slodczyk, P. Colomban, N. Malikova et al., *Solid State Ionics* (2013) in press.

[14] A. Meyer, S. Stüber, D. Holland-Moritz et al., *Phys. Rev B* 77 (2008) 092201.

[15] D. I. Kolokolov, H. Jobic, A. G. Stepanov, et al., *J. Phys. Chem. C* 116 (2012) 15093–15098.

spectroscopy with good energy resolution covering large momentum transfer values are essential to address these questions. Another example is the investigation of solid oxide fuel cells (SOFC) where a detailed understanding of the frequency dependent proton conduction is still lacking. While standard quasielastic neutron scattering experiments only probe the static state, pump-probe like experiments with on-line coupling of an impedance spectrometer can also monitor the dynamic response. For electrolytes in general, electrical excitation is a way to observe the dynamical susceptibility and the coupling to inelastic neutron scattering experiments will yield new insights for performance improvements. For most functional materials it is not only necessary to investigate the starting and the final conditions but important knowledge can be gained from the intermediate transient stages, especially since material development often implies understanding and refining the processing parameters. Consequently, it is often desirable to follow the ongoing reactions as function of time after preparation of a defined starting point or after a dedicated stimulus such as e.g. temperature step, gas pressure or electric fields. Another example are catalysts frequently added to facilitate (or even enable) a desired reaction path. Here, the mode of operation is often only poorly understood. The high flux, the good signal-to-noise ratio and the large dynamic range of the proposed instrument enable to follow kinetically controlled reactions and thus bring further advances in materials development.

Magnetic Materials

Understanding and manipulating magnetic materials on a microscopic scale has a huge impact on technological applications as well as fundamental science. Of special interest are for instance charge and spin ordering in multiferroica, or the symmetry changes observed in the spin dynamics in high temperature superconductors. To further understand these phenomena and to benchmark theory with experimental results neutron spectroscopy is the ideal tool to provide excitation modes on various length and energy scales. Further areas of applications include molecular magnets which can be used in such diverse fields as e.g. spintronics for ultra high density magnetic recording or biological applications.

The successful experiment in any of these fields depends on high intensity, a clean resolution function, excellent signal-to-noise ratio, and a large as possible dynamic range. The proposed instrument will have the necessary capabilities to be able to bring significant progress in both fundamental science and technological application, especially in the above listed areas of interest. The chopper system of the instrument enables to focus on the time domain of interest by choosing the appropriate energy resolution. The wavelength range of 2.5 Å covered in multi-energy mode ensures that significant parts of $S(q,\omega)$ are mapped simultaneously. The guide system is optimized for maximum flux for cold neutrons while it will also have significant transport in the thermal regime (down to 1 Å). The guide layout avoids the direct line-of-sight for an improved signal-to-noise ratio. Most experiments are expected to utilize the standard guide configuration with an extended beam spot size of 20 x 40 mm^2 at the sample position. The homogenous beam profile and the divergence of +/- 1 deg is suitable for large samples areas as they are typically necessary for hydrogen containing materials in order to minimize multiple scattering effects, or for single crystal magnetic studies. The focusing option can be employed to reduce the beam spot size to 10 x 10 mm^2 (at 5 Å incoming wavelength) with an increase of intensity up to a factor of 3 and will best be suited for dedicated sample environments and small sample sizes. With the tendency to increase sample complexity in order to approach more realistic scenarios and thus technologically more relevant experiments, the demand for a powerful, high performing cold chopper spectrometer will remain very high. Especially, it is expected that the number of experiments that use multi energy mode will increase, for the benefit of the inherently

guarantied identical sample conditions of the simultaneously probed parts of $S(q,\omega)$ and increased measurement speed and. The former is especially important for time resolved measurements, or if the sample conditions are likely to change during extended measurement periods. Similarly, it is expected that simultaneous secondary characterization of samples at the beam line (e.g. Raman or infra-red spectroscopy) will be further increasing. Examples include e.g. pump-probe experiments on biological molecules for photosynthesis, H_2 adsorption in porous materials for hydrogen storage or CO_2 sequestration or the dynamics of Li-conducting electrolytes (e.g. ionic liquids) under electrical stimulation in a battery.

All these type of experiments require a high performance instrument with tuneable energy resolution and good signal-to-noise ratio. Today, the operating cold chopper spectrometers both on spallation and reactor source (such as e.g. IN5, LET, CNCS, Amateras, TOFTOF, …) are high in demand with more beam time days requested than available for allocation (with typical overbooking factors >3) and it is not expected to change in the coming years. Moreover, we anticipate that an increasing number of biological driven applications will benefit from spectroscopy experiments, partly due to the fact of more powerful spectrometers adapted to the need of biological samples and partly due to advances in sample preparation, deuteration techniques or crystal growth. In conclusion, the user base for a cold chopper spectrometer is likely to become even larger compared to today and the proposed instrument will be of great use for the community.

The current other chopper spectroscopy instrument propositions for the ESS are a bispectral chopper spectrometer specialized to the mapping of magnetic excitations (with a length of 150 m) and a short, high flux cold chopper spectrometer dedicated to the exploration of a wide dynamic range. With the focus on disordered systems with medium to high energy resolutions, the proposed cold chopper spectrometer will be a significant contribution to the instrumentation suite of the ESS. With the ongoing high demand of chopper spectrometer beam time the new cold chopper spectrometer is essential for a broad user community, ranging from biology to quantum phenomena.

1.2   Description of Instrument Concept and Performance

General layout

The scientific drivers outlined above require an instrument with medium to high energy resolution in the range of $\Delta E/E = 3 - 1\%$, an excellent signal-to-noise ratio and a dynamic range that should at least probe one order of magnitude (in time domain) to be able to disentangle the various relevant motions. The q-range should cover low values (0.05 Å^{-1} ≤ q) needed for large scale structures which are typical for biological and soft condensed matter samples. On the other side, large q-values (q ≤ 10 Å^{-1}) are mandatory for material science questions as for example for host-guest systems. The majority of experiments is expected to take place at an energy resolution of 3 % (i.e. 100 μeV [16] at $\lambda = 5$ Å) and the instrument is optimized for maximum flux at these settings. However, the energy resolution can be freely tuned by the chopper operation parameters in the range $\Delta E/E = 6\%$ - 1%. To achieve a 3 % energy resolution, the source pulse needs be shaped, and the opening time τ_P should

---

[16] Report of the ESS workshop *Science Visions for the Europaen Spallation source – German Perspectives*, Bad Reichenhall 10.-12.10.2012

ideally be not be larger than 1000 µs (FWHM of a triangular shaped pulse) in order to minimize effects of the asymmetrically shaped edges on the final resolution function. Under these conditions, the optimum distance L_{PM} of the pulse shaping and the monochromatizing chopper is 108 m, yielding a total instrument length of 120.4 m. The natural wavelength band of the instrument is 2.5 Å which is sufficient to probe a significant part of S(q,ω) during one single measurement. A schematic sketch of the instrument is given in Figure 1. With the science questions in focus, the instrument is optimized for cold neutrons and it will face the cold moderator. The guide system will have two configurations, i.e. to accommodate hydrogenous materials that require a large beam size but homogenous flux distribution and a focusing option for small samples. The former setting is also very well suited for single crystals and magnetic studies, while the latter option will be beneficial for samples that can only be produced in small quantities or when restrictions due to the sample environment apply (e.g. pressure cells, etc.). This will be realized by an exchangeable guide section after the FO/M-chopper system.

The utilization of the pulse in the available source-pulse time frame is illustrated in Figure 2. The pulse shaping chopper pair selects a slice of the source pulse (depending on the desired energy resolution) which will be delivered to the FO/M-chopper system at 115 m. Two band width choppers (BW_1/BW_2) ensure that no frame overlap or cross talk between successive source pulses occurs. The FO/M-chopper system is used to set the resolution and the operation mode, i.e. to select the number of pulses impinging on the sample. In this manner, for each scientific question, the optimum instrument settings for resolution, dynamic range and flux can be chosen. Especially, the low resolution – high flux mode will be optimized for kinetic measurements while e.g. the entanglement of different dynamic processes in soft matter or biological samples will benefit from the medium to high resolution setting of the instrument.
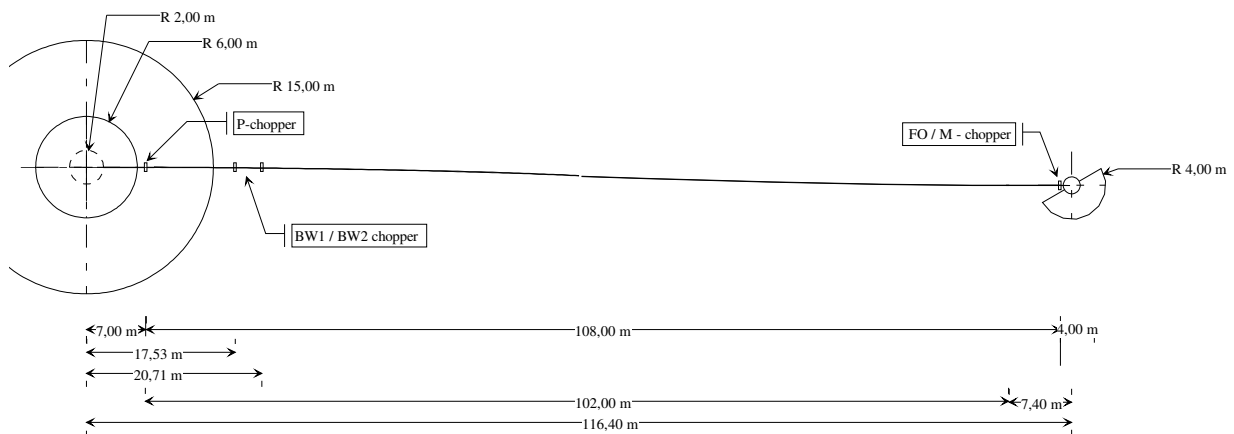

Figure 1: Schematic layout of the instrument. The P-chopper is located at 7 m just after the monolith and the FO/M-chopper system is positioned at 115 m from the source. The position of the BW_1 / BW_2 choppers is generic. The sample will be positioned at 116.4 m, and the secondary spectrometer consists of a 4 m flight path. The guide system avoids the direct line of sight from the source.
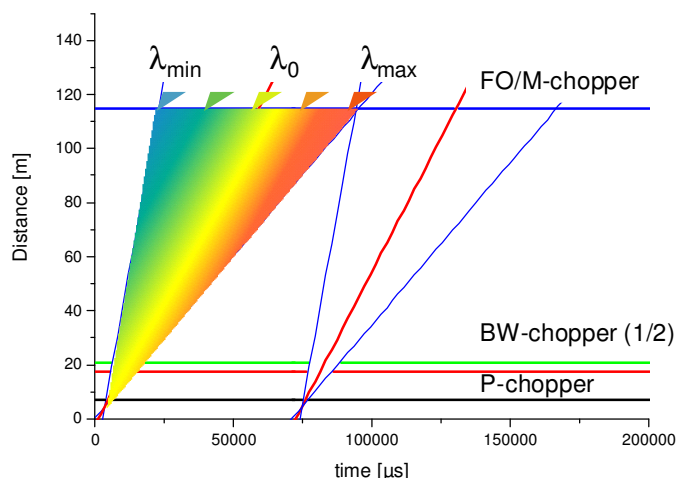
Figure 2: Time-distance diagram of the instrument. The pulse shaping chopper pair selects a slice of the source pulse (depending on the desired energy resolution) which will be delivered to the FO/M-chopper system at 115 m. Two band width choppers (BW_1/BW_2) ensure that no frame overlap or cross talk between successive source pulses occurs. The FO/M-chopper system is used to set the resolution and the operation mode, i.e. to select the number of pulses impinging on the sample.

Primary and secondary spectrometer are designed to work in balanced conditions. The secondary spectrometer will have a flight path of 4 m and a detector angular coverage of -15 – 140°. The waiving of more angular coverage yields to easy access of the sample area which is important in view of specialized sample environments or secondary characterization of the sample on-line.

Chopper system

The chopper system consists of a cascade of seven chopper disks. The operation parameters are given in Table 1 and the functionality is as follows:

- Pulse shaping counter rotating chopper pair at 7 m and 7.025 m from the source (P-chopper). For a clean resolution function the time aperture will be restricted τ_P = 1000 µs (FWHM) to minimize effects from the asymmetry (in time) of the source pulse which eventually would be mirrored in the resolution function of the instrument. For high flux, low resolution measurements, the entire source pulse can be chosen.

- Band width chopper. The two band width (BW_1/BW_2) choppers prevent overlap and cross talk between subsequent source pulses without restricting the natural wavelength band of the instrument. Each rotates with the source frequency. For the McStas calculations the position were set to 17.53 and 20.71 m, respectively, but these are generic values which are not crucial for the instrument performance.

- Frame overlap chopper (FO) at 114.95 m: This chopper is located just in front of the monochromatizing chopper systems and is used to adjust the number of pulses (per source time frame) in multi energy mode. Its rotation speed is adjusted with the ratio R according to f_{FO} = (R-1)/R x N_2 x 14 Hz where (R-1)/R x N_2 is an integer value and f_M = N_2 x 14 Hz is the rotation speed of the M-chopper pair.

- Monochromatizing counter rotating chopper pair (M-chopper) at 114.975 and 115 m, respectively. This chopper pair is used to select the wavelength and energy resolution of the neutron beam. Typical time apertures are in the order of 10 - 100 μs thus requiring high rotation speed f_M. Depending on the settings of the FO chopper one or several pulses are impinging on the samples with wavelength $\lambda_1 < \lambda_2 < .. < \lambda_n$, arriving equally spaced in time. For higher flexibility of the energy resolution, two windows with different apertures (5° / 3°) are foreseen. The phase with respect to the FO-chopper (with only one window) is used to select the aperture.

Table 1: Chopper Parameters, specifiying position from the source, angular aperture and typical rotation speed.

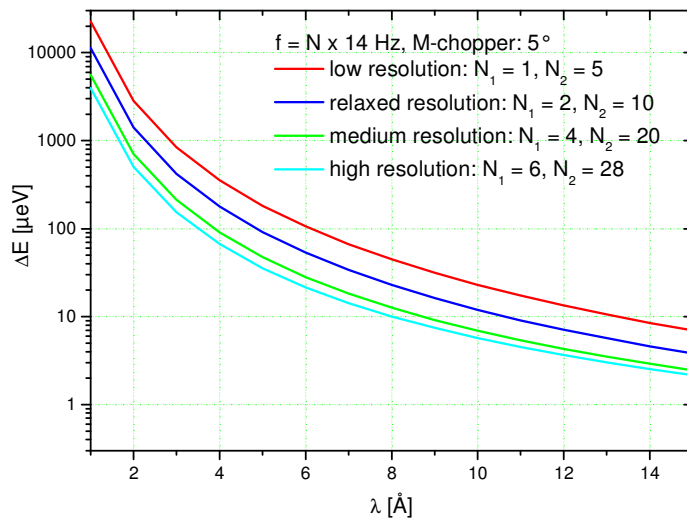| Chopper No	Position	Aperture	Rotation speed
P_1	7 m	14.67	N_1 x 14 Hz, N_1=1-10 (f_{max} = 140 Hz)
P_2	7.05 m	14.67	$-N_1$ x 14 Hz, N_1=1-10 (f_{max} = 140 Hz)
BW_1	17.53 m	28.58	14 Hz
BW_2	20.71 m	38.63	14 Hz
FO	114.9 m	5°	N_{FO3} x 14 Hz, N_{FO2}= N_2 x (R-1)/R
M1	114.95 m	5° / 3°	N_2 x 14 Hz, N_2 = 10-28 (f_{max}=400 Hz)
M2	115 m	5° / 3°	$-N_2$ x 14 Hz, N_2 = 10-28 (f_{max}=400 Hz)

Figure 3: Analytical elastic resolution for low, relaxed, medium and high energy resolution settings and an angular opening of the M-choppers of 5° (solid lines). The calculations assume a total path length uncertainty (detector and sample) of ΔL = 1 cm. A comparison with ΔL = 2 cm is shown in the annex, section 3.2)

The chopper settings and the analytically obtained energy resolution are summarized in Table 2 and illustrated in Figure 5. From $\lambda \geq 15$ Å, the energy resolution is dominated by the path length uncertainty ΔL of sample and detector. The energy resolution values for relaxed resolution mode (i.e. $N_1 = 2$, N_2= 10) are 91 μeV for $\lambda_0 = 5$ Å, while at $\lambda_0 = 9$ Å (i.e. $E_i = 1$ meV) 9 μeV energy resolution can be reached, as required by the science drivers. For ΔL= 20 mm, the pathlength uncertainty becomes already significant for $\lambda \geq 9$ Å (This is

illustrated in the annex, section 3.2). With the above used chopper settings, the wavelength band that arrives at the detector position is clean from frame overlap or cross talk from subsequent P-chopper pulses, as is shown by acceptance diagrams (see annex, section 3.1).

Table 2: Operation parameters, analytic elastic energy resolution (FWHM) and usable wavelength band. The elastic energy resolution is calculated for an M-chopper aperture of 5 °. For the calculation of the wavelength band, τ_{Source} = 4000 µs was assumed, the detector position is located at 120.4 m)

Resolution setting	N_1	N_2	ΔE (FWHM) [µeV] 2 Å M-chopper 5°	ΔE (FWHM) [µeV] 5 Å M-chopper 5°	ΔE (FWHM) [µeV] 9 Å M-chopper 5°	Wavelength band Δλ [Å]
Low	1	5	2836	182	31	2.47
Relaxed	2	10	1413	91	16	2.47
Medium	4	20	705	47	9	2.47
High	6	28	506	35	7.5	2.44

With an instrument length of 120.4 m, the natural wavelength band of the instrument is 2.5 Å (assuming τ_{source} = 4000 µs) hence in multi energy mode approximately one order of magnitude in energy resolution will be covered simultaneously (depending on the central wavelength λ_0). For high energy resolution (i.e. N_1 = 6), the wavelength band is restricted by the time aperture of the P-chopper and the minimum wavelength band is 2.44 Å. The accessible q-range varies with the incoming wavelength as shown in Figure 4. Assuming a minimum usable detector angle of 6 deg, at λ = 5 Å, a minimum q-value of 0.13 Å^{-1} is obtained already without small angle option, suitable for larger structures in the samples.

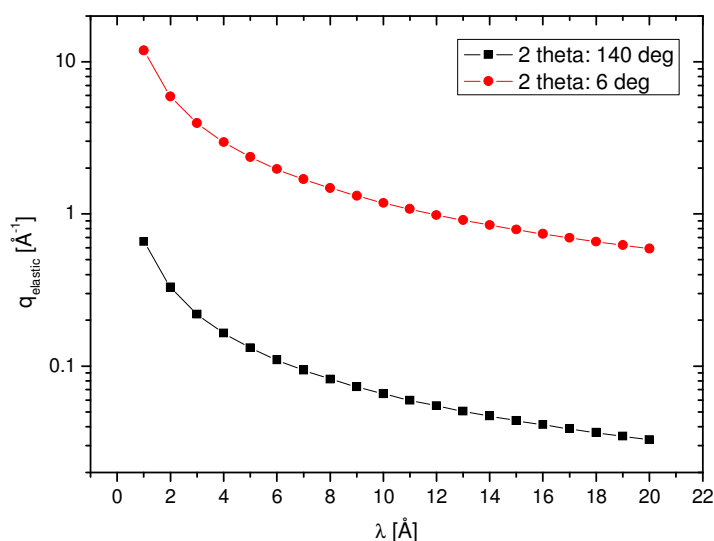Figure 4: q-Range of the instrument in dependence of the incoming wavelength λ for a detector angular range of 6 − 140°.

The (analytical) energy resolution as function of energy transfer that will be covered for different wavelength λ in relaxed energy resolution (N_1=2, N_2 = 10) is shown in Figure 5 while Figure 6 compares different chopper rotation speeds (λ_0 = 3 Å). In any experiment, a wavelength range of λ_0 +/- 1 Å will be covered and thus a mapping of the dynamic range.
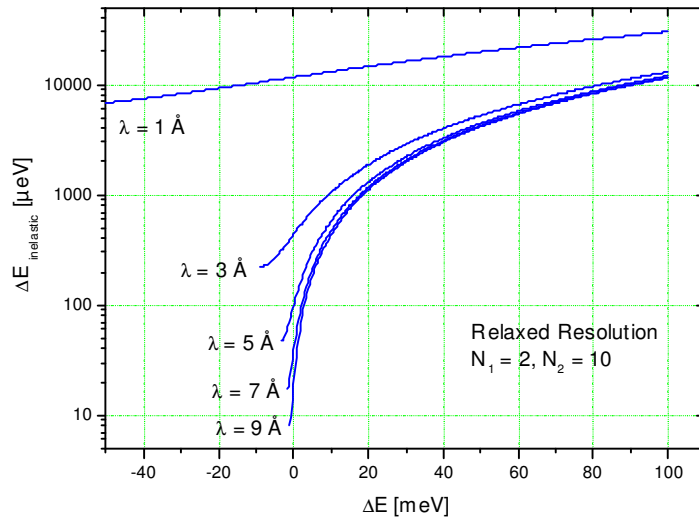
Figure 5: Energy resolution as function of energy transfer for relaxed resolution mode. In any experiment a wavelength range λ_0 +/- 1 Å will be covered.
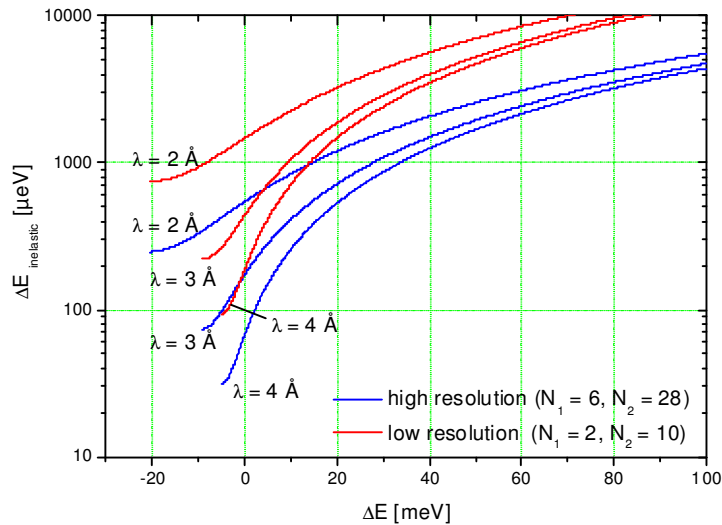

Figure 6: Energy resolution as function of energy transfer for relaxed and high resolution chopper settings, for measurements centred around λ_0 = 3 Å.

The performance of the instrument has been confirmed with Monte Carlo simulations for the various operation parameters as specified above. The elastic energy resolution was determined using a generic ideal incoherent elastic scatterer (vanadium like, diameter 20 mm, wall thickness 1 mm) using a McStas time-of-flight monitor positioned at a detector angle of 90°, the results are shown in Figure 7. (For $\lambda \geq 5$ Å and medium / high resolution

settings, a vanadium like-scatterer with 10 mm diameter was used.) The simulated results confirm the performance expected from the analytical calculations.
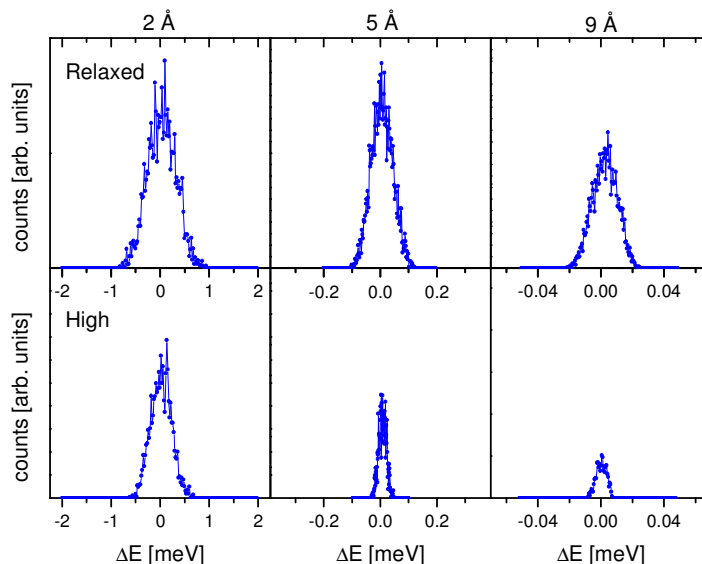

Figure 7: Elastic energy resolution for relaxed and high resolution chopper settings for λ = 2, 5 and 9 Å. (McStas

simulation, TOF2E monitor at the detector position at 90° scattering angle, scattering at a cylindrical ideal incoherent

elastic scatterer).

The chopper system is designed such that the entire permissible wavelength band will be delivered to the FO/M-chopper position. The number of pulses impinging on the sample and their difference in wavelength $\delta\lambda$ can be chosen be the operation parameters of the FO chopper. The instrument mode can be adjusted from single pulse option (i.e. λ_0) to multi energy mode with up to N_2 pulses per source pulse (where $f_M = N_2$ x 14 Hz is the M-chopper rotation speed). In general, the FO chopper will rotate with a frequency (R-1)/R x N_2 and thus the difference compared to f_M corresponds to a multiple of 14 Hz. As the FO and M-chopper will be positioned as close as possible [17] a sequence of pulses is generated that is equally spaced in time with wavelength $\lambda_0 \pm$ n·$\delta\lambda$ (n = .., -2, -1, 0, 1, 2, ..). λ_0 is the central wavelength in the wavelength band. The equal distance of $\delta\lambda$ for subsequent pulses is strictly true only for a point source. For the extended pulse of the ESS, different parts of the source pulse are probed as the wavelength band is scanned at the detector position. This is further explained in the annex, section 3.3, but this correction does not compromise the performance of the instrument in any way. The choice of ratio determines the separation in time. It can be adjusted to fit experimental requirements in order to avoid overlap between subsequent pulses. Importantly, for each setting of the ratio, the full band width of the instrument will be utilized and thus large parts of S(q,ω) will be mapped simultaneously in multi energy mode.

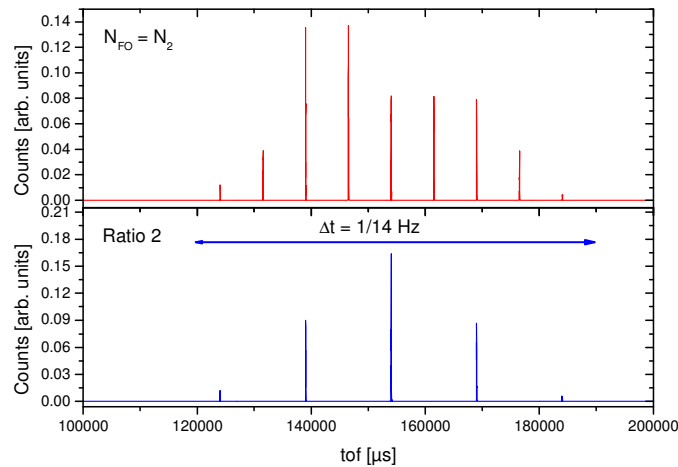[17] For all simulations, the space between adjacent disks was assumed to be 25 mm.

Figure 8: Time-of-flight monitor at the detector position (2th = 90°) for relaxed resolution (N_1 = 2, N_2 = 10) in multi energy mode, for N_2 pulses (upper panel) and Ratio 2 (lower panel). Scattering from a generic ideally incoherent scatterer. Each of the pulses can be analysed separately, the wavelength band $\Delta\lambda$ between the shortest and longest wavelength that probe the sample is ~2 Å, the central wavelength is λ_0= 5 Å.

This is illustrated in Figure 8 where the sequence of pulses is shown for two different ratios (measured at the detector position after scattering at a vanadium like scatterer at a 90° scattering angle). While the theoretical gain due to multiple E_i is 28 at maximum (for f_M = 28 x 14 Hz) when comparing single pulse to multi-energy mode, it is expected that the majority of experiments will utilize 5 – 10 pulses to fill the source pulse time frame.

The flux at the sample position (obtained from McStas calculations) for the various energy resolution settings is summarized in Table 3. The given numbers are for λ_0. The flux exceeds current state of the art cold chopper spectrometers by at least a factor of 2 (at comparable resolution settings, i.e. IN5: $6.3 \cdot 10^5$ n /(s cm^2) for 5 Å for ΔE = 100 µeV, LET = $5 \cdot 10^4$ n /(s cm^2 at $\Delta E/E$ = 2%) already in the single pulse option. Utilizing the multi energy mode, the instruments true capabilities will become apparent with gain factors of 10-20 (assuming 5 – 10 pulses in multi energy mode) compared to existing instruments.

Table 3: Energy resolution measured from McStas simulations by scattering from a generic ideally incoherent scatter (cylindrical rod, 20 mm diameter, 1 mm thickness, for the medium and high resolution setting a 10 mm rod was used). The detector was positioned at a 90° angle, and infinitely thin. Also given is the flux obtained at the sample position for the various resolution settings.

Chopper settings	ΔE (λ_0 = 2 Å) [µeV]	Flux (λ_0 = 2 Å) [n /(s cm^2)]	ΔE (λ_0 = 5 Å) [µeV]	Flux (λ_0 = 5 Å) [n /(s cm^2)]	ΔE (λ_0 = 9 Å) [µeV]	Flux (λ_0 = 5 Å) [n /(s cm^2)]
N_1 = 1, N_2 = 5	2630	$3.9 \cdot 10^6$	184	$5.94 \cdot 10^6$	32	$1.1 \cdot 10^6$
N_1 = 2, N_2 = 10	775	$8.7 \cdot 10^5$	94	$1.5 \cdot 10^6$	20	$2.5 \cdot 10^5$
N_1 = 4, N_2 = 20	657	$3.8 \cdot 10^5$	43	$4.6 \cdot 10^5$	8	$6.3 \cdot 10^4$
N_1 = 6, N_2 = 28	512	$2.8 \cdot 10^5$	34	$2.8 \cdot 10^6$	8	$3.2 \cdot 10^4$

Guide system

The instrument will be facing at the cold moderator and the neutron guide will start inside the monolith at 2 m from the source with guide dimensions of 40 x 100 mm^2 and a coating m = 3. The schematic beam layout is shown in Figure 1. From the monolith, a straight guide section extends up to just after the P-chopper. At 8 m from the source, a long s-shaped section with m = 3 (total length = 101 m, radius = 2318.5 m) begins which brings the beam out of the direct line-of-sight, and already after 23 m from the source, the guide is out of the line-of-sight once. The guide dimensions are kept constant at 40 x 100 mm^2 as well as the guide coating. Compared to a straight guide, the neutron transport for the cold region ($\lambda \geq 2$ Å) is less than 10 % for the curved option with the here chosen radius. This radius yields an offset at the sample position of 1.1 m compared to the direct line of sight, and thus avoids also the direct view of the detector (with a maximum detector angle of -15 deg). From 109 m from the source, an elliptically shaped focusing section towards the sample begins and the guide layout was optimized under consideration of the required width at the FO-M /chopper position. The m-coating up to the FO/M-chopper system is kept constant at m = 3. The s-shape ensures a clean cut-off at 1.0 Å and a homogeneous beam profile at the exit of the bender section. Higher m-values were investigated, but for m ≥ 3 no significant gain in flux was obtained, while on the other hand, divergence was increasing (see annex, section 3.4). The final guide section after the FO/M-chopper system will be exchangeable to adapt for different experimental requirements, i.e. a homogenous 20 x 40 mm^2 beam spot with +/- 1 deg divergence for hydrogenous samples or single crystals and a focused beam spot 10 x 10 mm^2 for small sample sizes and for experiments that tolerate higher divergence. A schematic layout of the focusing end section is shown in Figure 9. The exchangable end piece for the focusing part is coated with m = 5. With these configurations, the flux of the white beam was determined in McStas simulations, the results are shown in Figure 10. The flux of the white beam is 2.2·10^9 n /(s cm^2 Å) at 5 Å for the standard configuration and 5.4 ·10^9 n /(s cm^2 Å) for the focusing option which is comparable to today's state-of-the-art instruments.
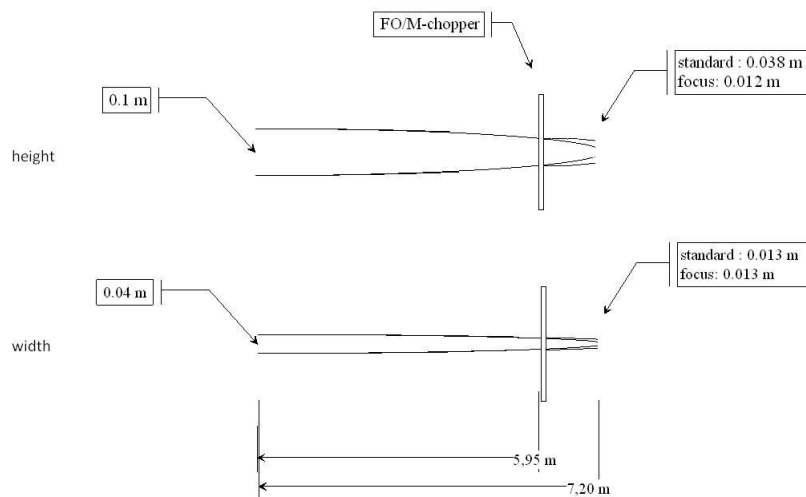

Figure 9: Schematic guide layout of the focussing end section towards the FO/M-chopper system and the exchangeable end section.
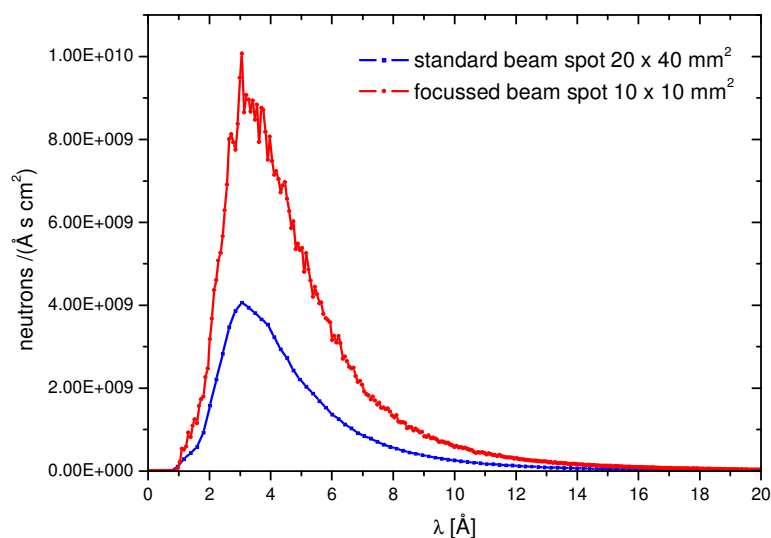
Figure 10: Flux of the white beam at the sample position (normalized to the beam spot size). From the standard guide end section to the focussing end section, an intensity gain of roughly 2-3 can be obtained per unit cm^2.

The two beam configurations are further illustrated in Figure 11 for $\lambda = 5$ Å, the beam extension in horizontal and vertical direction as well as the divergence for wavelength $\lambda = 2$, 5, and 9 Å are summarized in the annex, section 3.4. The standard nose delivers an extended homogenous beam with a divergence of +/- 1 deg. For dedicated sample environments, small sample sizes the beam spot can be chosen to be about 10 x 10 mm^2.
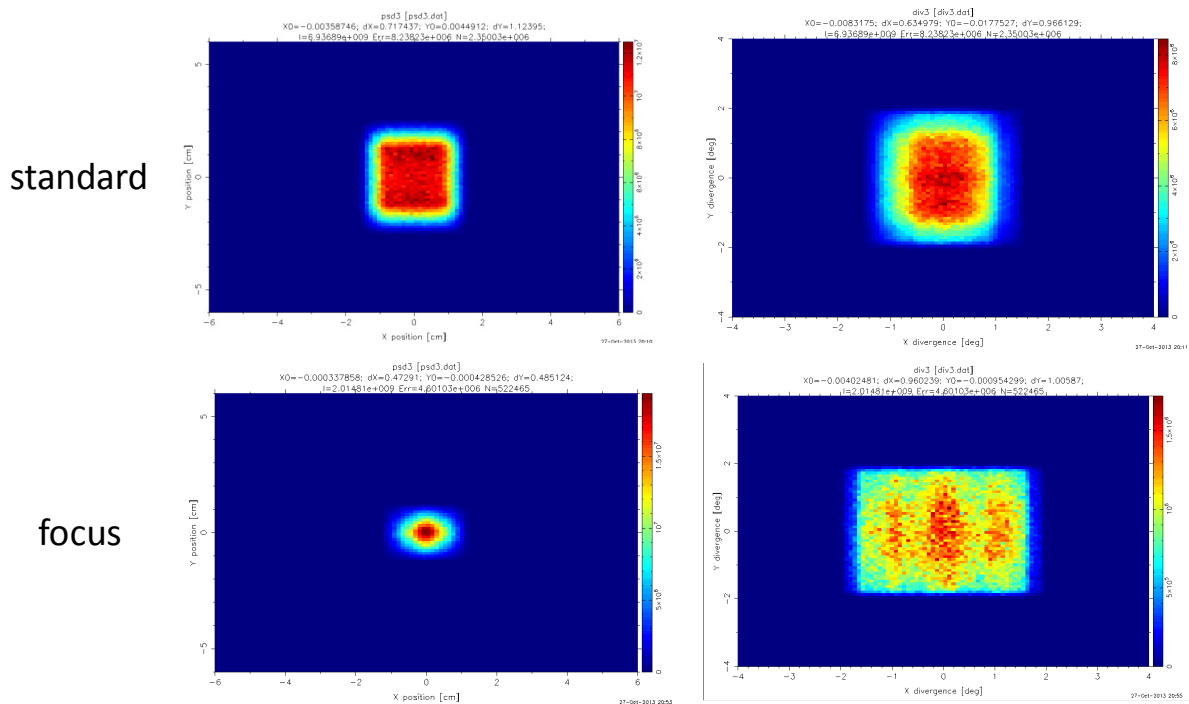

Figure 11: Beam profile (left panel) and divergence (right) for the standard and focused beam configuration for $\lambda_0 = 5$ Å.

Focusing of the beam works best at for $\lambda \leq 5$ Å and here gain factors (normalized to unit cm^2) of 2-3 can be expected compared to the standard beam layout.

The performance of an s-bender guide was compared to an elliptic guide solution (with a kink at 7 m from the source, to avoid direct line-of-sight). It was found that the performance of the s-shaped bender guide with a converging section at the end is compatible with an elliptic guide solution for the intended wavelength and divergence regime while it will be less expensive. Therefore, the s-bender solution is favored.

Secondary Spectrometer

The secondary spectrometer will have a 4 m flight path and the detectors will cover an angular range of -15° – 140° horizontally and +/- 20 deg in the vertical direction (total detector height: 3 m). Using only one side for the detector coverage, the side access to the sample area will be approximately 60° thus facilitating the installation of non-standard sample environments. The pixel size of the detector will be at minimum 25 x 25 mm^2 to enable mapping of $S(q,\omega)$ with high q-resolution [18]. Moreover, the arrangement of the modules should minimize dead angles in the detector coverage. The detector thickness (and hence the corresponding time uncertainty of the neutron time-of-flight) needs to be in the order of 10 mm in order to not compromise the energy resolution performance of the instrument. The detector vessel will be evacuated. With the shortage of ^{3}He gas detector tubes, currently foreseen are ^{10}B converter layer gas detectors which are still under development. Data acquisition will be done in event mode.

Shutters

The guide layout insures that there is no direct-line of sight from the source to the sample position. With only a light shutter in the monolith, the instrument concepts foresees an heavy shutter and an additional light shutter, both positioned after the P-chopper inside the bunker that extends 15 m from the source. In this way, safe access to the sample position is given. The heavy shutter ensures that with running source, all instrument components (after the P-chopper pair) can be closed from the neutron beam which is beneficial for maintenance and repairs. No T_0-chopper is foreseen.

Summary

With the flexible energy resolution and a usable wavelength band of 2.5 Å, the instrument is ideally suited to address the science drivers outlined in section 1.1. With a flux that is at least a factor of 2 higher compared to IN5 and existing instruments (for a single pulse and comparable resolution) and a wavelength band of 2.5 Å accessible in multi-energy mode, gain factors of the order of 20 are expected in comparison with existing instruments which makes kinetic studies and pump-probe experiments are real possibility. The guide layout ensures low background and its two end section can be used to adjust the beam profile to the experimental requirements. In summary, the key parameters of the proposed instrument are as follows:

---

[18] The divergence of the here proposed guide system will only require a pixel size of 50 x 50 mm, however in view of single crystal work the detector angular resolution is chosen to fit a better collimated beam.

Moderator:	cold source
Moderator – sample distance:	116.4 m
Wavelength range:	1.0 – 20 Å
Energy Resolutions: $\Delta E / E =$	1 – 6 % (34 μeV – 184 μeV @ 5Å)
Q-range /Resolution:	@ 2 Å: 0.32 – 5.90 Å^{-1}
	@ 5 Å: 0.13 – 2.36 Å^{-1}
Flux at sample @ 5 Å :	standard: $2.2 \cdot 10^9$ neutrons /(s cm^2 Å) white beam
	focus: $5.4 \cdot 10^9$ neutrons/(s cm^2 Å) white beam
Flux at sample, $\Delta E /E = 3$ %	2 Å : $8.7 \cdot 10^5$ neutrons /(s cm^2)
	5 Å : $1.5 \cdot 10^6$ neutrons /(s cm^2)
	9 Å : $2.5 \cdot 10^5$ neutrons /(s cm^2)
Beam size at sample:	standard: 40 x 20 mm^2
	focus: 10 x 10 mm^2
Divergence at sample (standard):	+/- 1 deg
Sample – detector distance:	4 m
Detector technology:	^{10}B converter layers
Detector coverage:	-15 – 140 deg

Add-Ons

Polarization / Analysis: Both, magnetic as well as quasi elastic measurements benefit from the possibility to polarize the beam and analyze its spin state after scattering. The brightness of the source makes this feature a real possibility. Polarization analysis is not foreseen as a day one feature of the instrument, but the instrument technical design will take a future upgrade into consideration, i.e. in the choice of materials for sample and detector vessel, and space for polarizer and analyzer components.

Small angle option: To probe large dimensions in real space as frequently seen in soft matter research, measurements at low q-values are necessary. Therefore, the possibility to include a small angle detector is foreseen as an exchange option for the ^{10}B converter layer module in forward direction and a the exchange guide will be equipped with a collimator to guaranty the necessary low divergence.

Adaptable Optics: In order to optimize the intensity for wavelength $\lambda \geq 4$ Å, it is planned to include an adaptable optics device with adjustable curvature which can then the set for the optimum performance at the chosen central wavelength λ_0.

1.3   Technical Maturity

Overall the instrument concept is based on established and mature components as well as proven concepts. However, this does not include the detector technology.

For the chopper system, the operational parameters for the P- and BW_1/BW_2 - choppers are non-demanding with rotation speeds of 14 – 140 Hz at maximum. The FO/M-chopper system will require higher rotation speeds with opening times up to 10 µs for the high resolution mode. Assuming a 70 mm diameter counter rotating disk system, this can be achieved with a 2.54° window aperture and rotation speeds of 330 Hz. With these settings, a 28 mm guide opening is obtained (at half height of a 70 mm window aperature). This is within the specification for currently available chopper disks (although at the high limit) [19]. For a 60 mm disk (and the same guide opening), the rotation speed needs to be 392 Hz to achieve the same opening time. (The setting was assumed for all McStas simulations in high resolution mode). This technology still needs to be developed for the use in a chopper spectrometer. Destructive tests of prototype disks made of carbon reinforced plastic with 60 mm diameter yielded an ultimate rotation speed of ca. 450 Hz (27.500 rpm) at which the disk is destroyed. Allowing for a 10 % safety margin, operational speeds at 400 Hz seem to be well possible within the near future. However, the instrument performance will not depend on the chopper development as a 70 mm diameter chopper disks are available and can be used. In view of the science drivers that push the instrument development, all of the scientific areas can be addressed in excellent manner and thus the instrument performance would not be compromised. The smaller disk size with higher rotation speeds is nevertheless preferred for the multi energy mode, since the maximum number of pulses is given by N_2.

During operation, the chopper disks will operate with very different frequencies which will require that the phase will be set in reference to a common master clock. Moreover, the functionality of the FO/M-chopper system requires that the three choppers are closely spaced. For the MsStas simulations, a spacing of 25 mm between adjacent disks was assumed which proved sufficient for the intended purpose. The commercially available three chopper systems can be made using this spacing.

The guide concept foresees a s-bender guide followed by an elliptic focusing section. The guide coating is kept constant at m = 3 throughout the entire length, except for the exchangeable final section after the FO/M-chopper system which will require m = 5. The maximum guide dimensions will be 40 x 100 mm^2. For the McStas simulations, the guide was build of linearly tapered segments and we suppose that only for last meter in front of the FO/M-chopper system and after the chopper system, a truly curved guide will be advantageous compared to the segmented one. The guide concept is therefore based on proven technology and there is no major risk attached to the realization of the instrument concept.

The biggest unknown for the instrument performance is the development of the detector technology. This is common for all ESS instruments that require a large area detector. With the shortage of ^{3}He-gas, the proven ^{3}He-gas detector tubes will (most likely) be either unavailable or prohibitively expensive. For the performance of the instrument, the key factors for the detector development are the efficiency of neutron detection, the depth resolution (and thus the neutron flight path uncertainty) of the detector (preferentially 10 mm), the lateral pixel size resolution which is mandatory for single crystal work (25 mm x 25 mm) and the detector induced background due to the amount of material in the beam. Recent tests of prototype modules at IN6 of the ESS detector group [20] show encouraging

---

[19] Astrium, to be used at SANS1, FRM 2
[20] Richard Hall-Wilton, IKON 4, Lund (2013)

results and it is expected that the ^{10}B-layer detector technology will advance adequately to be used in the first ESS instruments. With the multi-blade arrangement chosen for the prototypes the efficiency for neutron detection is 64 % (compared to 82% for ^{3}He at 5 Å [20]) in the relevant cold neutron region. Moreover, the current prototypes have the required pixel and depth resolution (10 mm), but the biggest uncertainty is the detector induced background which was observed in the first tests. In comparison to the ^{3}He tubes installed alongside in the experiment, the background signal was an order of magnitude higher which would make it impossible to follow weak signals. For the scientific challenges at hand, the signal-to-noise ratio is decisive for the success of any experiment. Without the necessary improvements on the detector technology, the performance of the instrument will be seriously compromised and ^{3}He would be the best solution if it would be available at a competitive price.

All other components have requirements that can be met by currently existing technology, such as vacuum vessels and equipment, motors for the exchange guide and slit systems. However, depending on the final layout of the ESS buildings, monolith and bunker special solutions for access to the components have to be found. For the proposed instrument, this concerns mainly the P-chopper system and the guides and shutters inside the bunker.

1.4   Costing

The estimated total cost is summarized in Table 4. The cost estimation was done according to ESS guidelines, further details of the costing are given in the following. The project will be conducted phases, i.e.:
> Year 1-3: engineering design and planning
> Year 2-4: final design
> Year 2-4: installation and procurement
> Year 2-4: cold commissioning and beam testing.

The costs are broken down in the following categories:
Integrated Design and System Integration: The total staff effort is estimated to be 144 PM (corresponding to a Lead scientist, design engineer and draft engineer for four years), the allocation to phase 1 to 4 is specified in Table 4. Costing of a person-month according to ESS guidelines is 10 KEUR /person-month. This topic comprises all the staff efforts, hence in the following only the hardware costs are specified.

Detectors: The cost estimate given be the detector group for a 50m^2 detector (i.e. for "full" angular coverage) for a cold spectrometer was given to be 8000 kEUR. With the lower angular coverage (~32 m^2) of the proposed instrument the estimated detector cost is:
> Detector(incl. Electronics, installation):   5120 kEUR.

Choppers: The P- and BW chopper are low frequency with non-demanding window apertures whereas the FO/M-chopper system requires high frequencies and development work. The total cost is estimated to:
> P/BW-chopper: 4 x 150 kEUR =   600 kEUR
> FO/M-chopper: 3 x 180 kEUR =   540 kEUR
> Sum: 1140 kEUR

Optical components: For the guide system a s-shaped bender section with m = 3 is proposed which will be considerably less expensive than elliptic guides with higher m-values, and the cost per meter of this guide was estimated to be 20 kEUR (neutron optics group FRM2), whereas the ellipitc focussing section will be more expensive. In total we estimate:

```
s-bender: 110 m x 20 kEUR /m =        2200 kEUR
elliptic / exchange: 9 x 30 kEUR/m =   240 kEUR
Radial collimator:                     500 kEUR
Sum:                                  2940 kEUR
```

Shielding: The shielding along the guide is estimated to be ~2.5 m^3 concrete/ meter of guide: Additionally, a heavy and a light shutter are foreseen. The total cost is estimated to:

```
shielding: 100 guide x 2.5m³ x 5 kEUR: 1250 kEUR
shutters and beam stop                  120 kEUR
Sum:                                   1370 kEUR
```

The shielding of the bunker is not finalized yet, and costing will be done by ESS, hence these costs will add to the final instrument budget.

Detector vessel: The vacuum vessel for the detectors, including pumps, windows, mounting and installation, the sample chamber and standard sample environment necessary for the day one operation (cryostat, oven, magnet):

```
Vessel:                         3000 kEUR
Sample stage and environment     700 kEUR
Sum:                            3700 kEUR
```

Instrument Specific Support Equipment: Additional costs that are included in any of the points above are:

```
Infrastructure
(cables, cooling water lines etc):   400 kEUR
Instrument crane:                     20 kEUR
Instrument hatch, office equipment    50 kEUR
Sum:                                 470 kEUR
```

Table 4

	Phase 1: Design + Planning		Phase 2: Final Design		Phase 3: Procurement and Installation		Phase 4: beam testing and cold commisioning		Total	
	year 1-3		year 2-4		year 2-4		year 3-4		year 1-4	
	PM	cost [kEUR]	PM	cost [kEUR]	PM	cost [kEUR]	PM	cost [kEUR]	PM	cost [kEUR]
Integrated Design	24	240	24	240	60	600	24	240	132	1.320
System Integration	3	30	3	30	3	30	3	30	12	120
Staff effort									**144**	**1.440**
Hardware										
Detectors -data aquisition										5120
Optical components										2940
Choppers										1140
Detector vessel and pumps, sample environment										4200
Shielding										1370
Instrument specific support										470
Total Hardware										**15.240**
Total (Hardware + Staff)										**16.680**

2.   LIST OF ABBREVIATIONS

Abbreviation	Explanation of abbreviation
λ	Wavelength
τ_M	Opening time of monochromating chopper
τ_P	Opening time of the pulsing chopper
BW-chopper	Bandwidth chopper
E_i	Energy of the incoming neutron
ESS	European spallation source
FO-chopper	Frame overlap chopper
FWHM	Full width half maximum
M-chopper	Monochromatising counter rotating chopper pair
N_1	Pulsing chopper speed in multiples of 14 Hz, i.e. N_1 x 14 Hz
N_2	Monochromating chopper speed in multiples of 14 Hz, i.e. N_2 x 14 Hz
P-chopper	Pulsing counter rotating chopper pair
R	Ratio of Frame overlap chopper
$S(q,\omega)$	Scattering function

PROPOSAL HISTORY

New proposal:	(yes/no)
Resubmission:	(yes/no)

3.   ANNEX

3.1   Acceptance Diagrams

The cleanliness of the pulse in terms of higher order contamination and cross talk between subsequent pulses was investigated using acceptance diagrams as described in Ref. [21]. The results for $N_1 = 2$ and $N_1 = 6$ are exemplarily shown in Figure 12 and Figure 13.
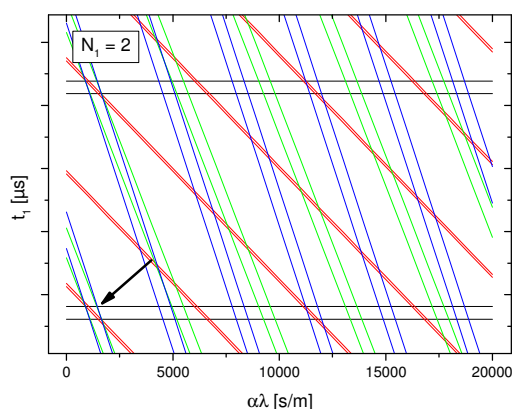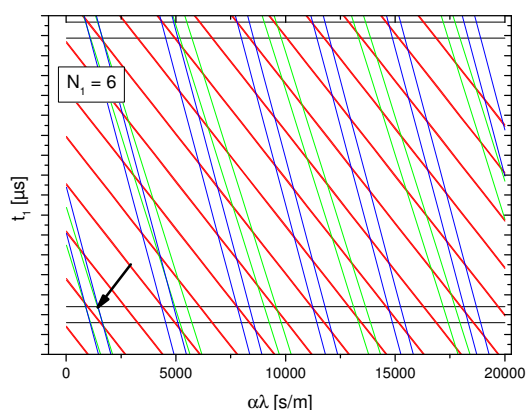

Figure 12: Acceptance Diagram for $N_1 = 2$. Shown are: opening of the source (black lines), opening of the BW_1/BW_2 chopper (blue and green lines) and the opening of the P-chopper for $N_1 = 2$. The counter rotating P-chopper is depicted as a 'single' opening time. The transmitted wavelength band (that will be delivered to the FO/M-chopper system) is given by the area where all openings lines intersect (marked by the black arrow). The central wavelength was $\lambda_0 = 5$ Å.

Figure 13: Acceptance Diagram for $N_1 = 6$. Shown are: opening of the source (black lines), opening of the BW_1/BW_2 chopper (blue and green lines) and the opening of the P-chopper for $N_1 = 2$. The counter rotating P chopper is depicted as a single opening time. The transmitted wavelength band (that will be delivered to the FO/M-chopper system) is given by the area where all openings lines intersect (marked by the black arrow). The central wavelength was $\lambda_0 = 5$ Å.

[21] J.R.D. Copley, Nuclear Instruments and Methods in Physics Research A 510 (2003) 318-324.

MXType.Localized
Document Number   MXName
Project Name   <<C-SPEC>>
Date   31/10/2013

The wavelength band (around the central wavelength λ_0 = 5 Å) that is transmitted to the FO/M-chopper system is marked by the black arrow. The acceptance diagram confirms that the spectra is clean up to $\alpha \cdot \lambda$=20 000 s/m, i.e. cross talk and contamination from subsequent pulses up to $\lambda \geq 80$ Å is suppressed. The acceptance diagram for N_1 = 6 also demonstrates the necessity of two band width choppers, otherwise cross talk between subsequent p-chopper pulses might occur.

3.2   Elastic Energy Resolution

The energy resolution depends on the chopper opening times (specified by the rotation speed and the window aperture) and the path length uncertainty. The minimum path length uncertainty will be 10 mm stemming from the detector, in realistic scenarios the sample extension will also play a role. The influence on the elastic energy resolution is illustrated in Figure 14 and Figure 15.
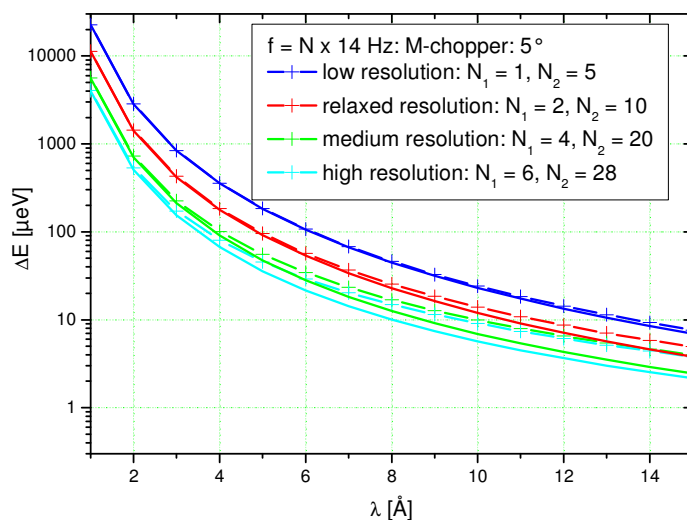

Figure 14: Analytic elastic energy resolution for a path length uncertainty of ΔL = 10 mm (solid lines) and ΔL = 20 mm (broken line). In high resolution mode and for wavelength $\lambda \geq \sim 5$ Å, the energy resolution is dominated by ΔL. For lower energy resolution settings of the chopper, ΔL does not have a significant influence.
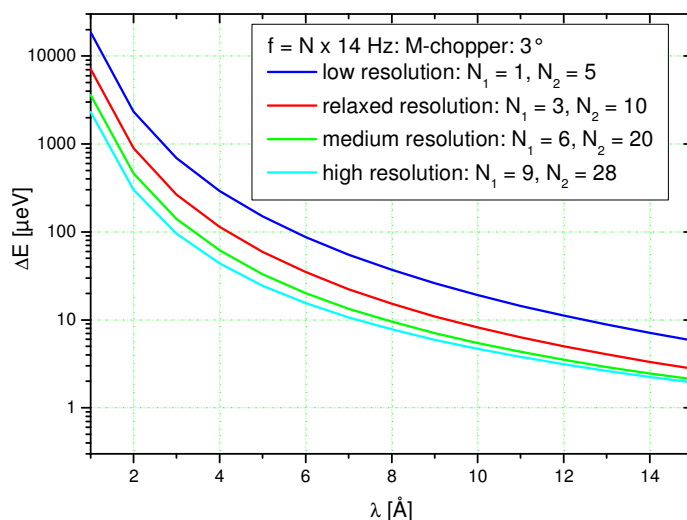
Figure 15: Analytical elastic energy resolution for high resolution mode with a M-chopper aperture of 3° (and balanced conditions for the P-chopper opening)

3.3   T_offset in multi-energy mode

In multi energy mode, the FO/M-chopper system is used to select a set of distinct wavelength from the oncoming wavelength band. For neutrons with the arrival time t_n at the M-chopper position, the effectively viewed part of the source pulse can be reconstructed. As t_n sweeps through the available time domain (given by the source frequency), different parts of the source pulse are viewed (see Figure 16). In any experiment, the chopper phase is selected such that the central wavelength views the source pulse maximum, i.e. the choppers will open at times $t_{ch}=\alpha \cdot \lambda \cdot L_{ch} + t_{offset}$, where L_{ch} is the distance of the chopper and the source and $\alpha= 252.77$ µs/(Å m). t_{offset} is chosen to be 1860 µs. The varying view to the source pulse implies that a corrected time offset has to be taken into account when calculating back the wavelength λ_n from the arrival time t_n at the detector position. Figure 17 shows the minimum and maximum time τ of the pulse probed as function of the neutron arrival time t_n at the detector (black dahed line), the corrected time-offset (taken as the average value of τ_{min} and τ_{max} and the corrected wavelength (symbols) in comparison to the ideal one (with t_{offset} = 1860 µs).
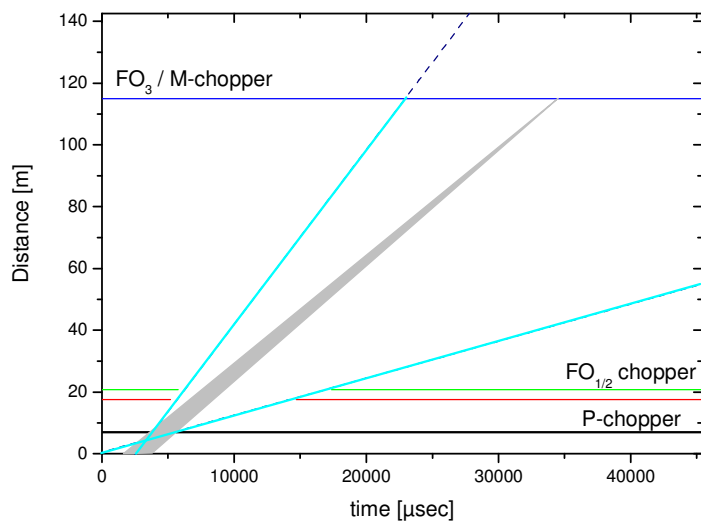
Figure 16: Time-distance diagram for the multi-energy mode. For neutrons arriving at time t_n at the M-chopper, the effectively viewed part of the source pulse can be reconstructed from t and the opening and closing time of the P-chopper t_{open} and t_{close}.
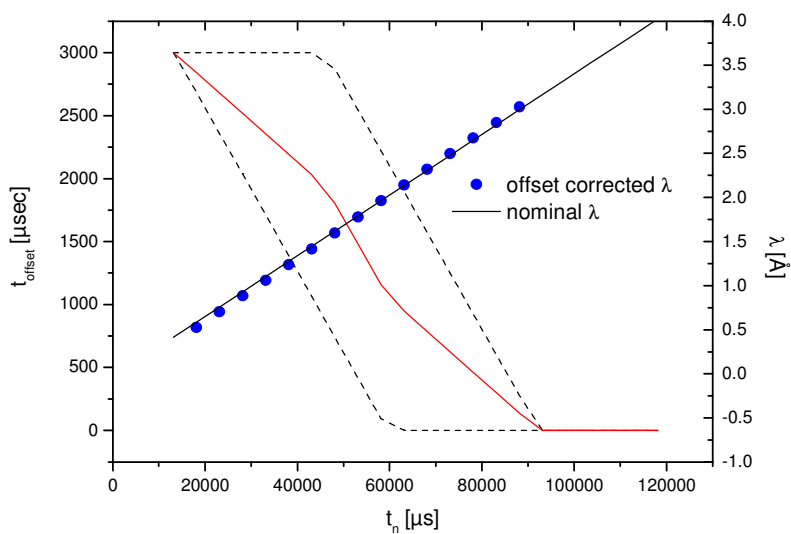

Figure 17: Time interval that is used from the source pulse as function of neutron arrival time t_n at the detector (dashed black lines), the corrected t_{offset} (red line) and corresponding wavelength λ_0

27(29)

3.4   Guide layout

The m-coating of the s-shape bender guide was chosen to be m = 3 throughout the entire instrument for the standard beam configuration with a 20 x 40 mm^2 homogenous beam spot.

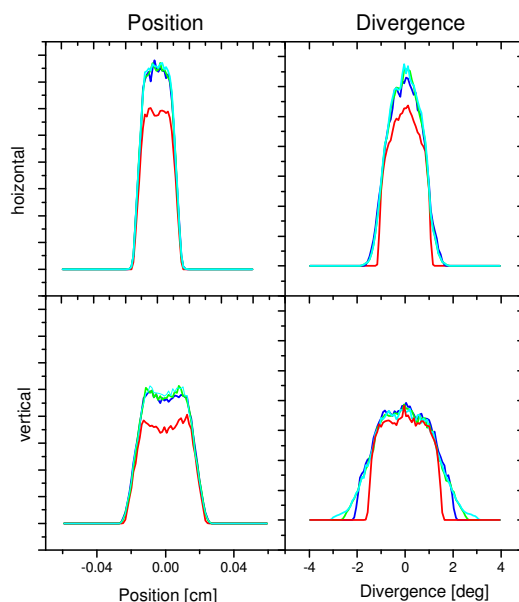Figure 18: Beam size and divergence at the sample position in dependence of the m-value of the guide coating for λ = 5 Å:

m = 2 (red), 3 (blue), 4 (green), 5 (cyan).

The beam spot size and divergence for the s-shaped bender guide is shown in Figure 18 for different m-values of the coating. While there is an intensity gain of about 25% when going from m=2 to m=3, further increase of the m-values only yields about 2% increase but at the expense of broader divergence. Therefore, an m-value of 3 was chosen for the guide layout.

The beam spot size and the divergence distribution for the standard beam configuration and the focusing option are shown in Figure 19 and Figure 20. For the focussing guide end section an m-coating value of m = 5 was used. For wavelength λ ≤ 5 Å, the beam size reduction works best and a factor (per unit cm^2) of 2-3 is gained in intensity for that wavelength band.
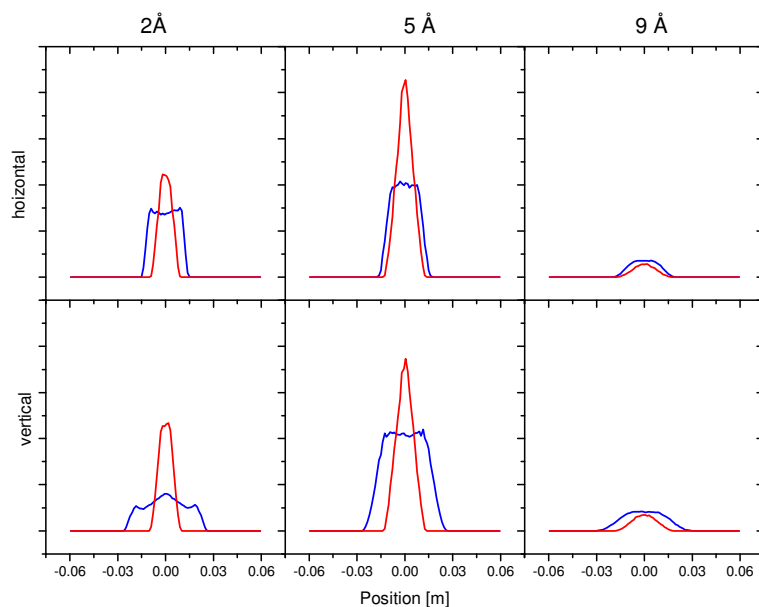
Figure 19: Beam spot size at the sample for the standard (blue) and focused guide configuration (red) for λ = 2, 5, 9 Å
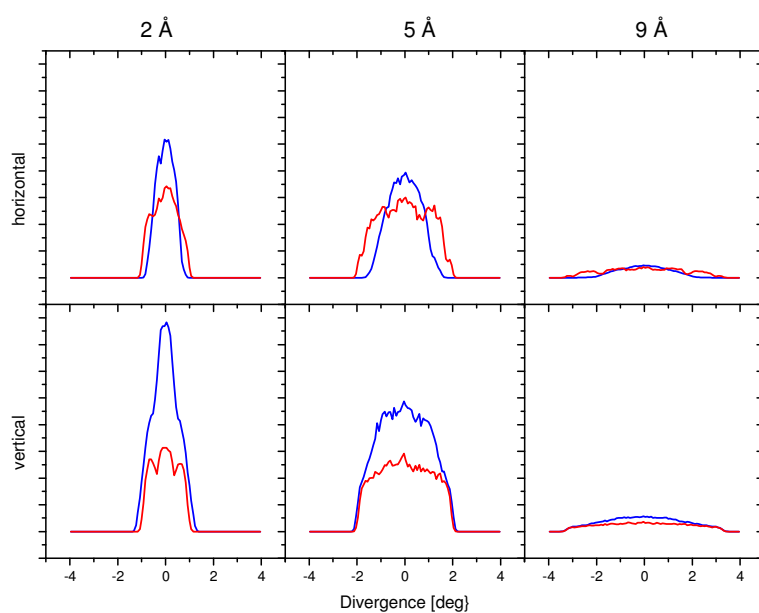

Figure 20: Divergence distribution for standard (blue) and focused beam (red) for horizontal and vertical orientation.